

Title: **Aerodynamic and Flow Characteristics of Tall Buildings with Various Unconventional Configurations**

Authors: Hideyuki Tanaka, Takenaka Corporation
Yukio Tamura, Tokyo Polytechnic University
Kazuo Ohtake, Takenaka Corporation
Masayoshi Nakai, Takenaka Corporation
YongChul Kim, Seoul National University of Technology
Eswara Kumar Bandi, Tokyo Polytechnic University

Subject: Wind Engineering

Keywords: Wind Loads
Wind Tunnel Testing

Publication Date: 2013

Original Publication: International Journal of High-Rise Buildings Volume 2 Number 3

Paper Type:

1. Book chapter/Part chapter
2. **Journal paper**
3. Conference proceeding
4. Unpublished conference paper
5. Magazine article
6. Unpublished

© Council on Tall Buildings and Urban Habitat / Hideyuki Tanaka; Yukio Tamura; Kazuo Ohtake; Masayoshi Nakai; YongChul Kim; Eswara Kumar Bandi

Aerodynamic and Flow Characteristics of Tall Buildings with Various Unconventional Configurations

Hideyuki Tanaka^{1†}, Yukio Tamura², Kazuo Ohtake¹, Masayoshi Nakai³,
Yong Chul Kim⁴, and Eswara Kumar Bandi²

¹Environmental Engineering Department, Takenaka Research & Development Institute, Takenaka Corporation, Chiba 270-1395, Japan

²Department of Architecture, Tokyo Polytechnic University, Kanagawa 243-0297, Japan

³General Manager, Advanced Structural Engineering Department, Takenaka Corporation, Tokyo 136-0075, Japan

⁴School of Architecture, Seoul National University of Science and Technology, Seoul 139-743, Korea

Abstract

Tall buildings have been traditionally designed to be symmetric rectangular, triangular or circular in plan, in order to avoid excessive seismic-induced torsional vibrations due to eccentricity, especially in seismic-prone regions like Japan. However, recent tall building design has been released from the spell of compulsory symmetric shape design, and free-style design is increasing. This is mainly due to architects' and structural designers' challenging demands for novel and unconventional expressions. Another important aspect is that rather complicated sectional shapes are basically good with regard to aerodynamic properties for crosswind excitations, which are a key issue in tall-building wind-resistant design. A series of wind tunnel experiments and numerical simulation have been carried out to determine aerodynamic forces and wind pressures acting on tall building models with various configurations: corner cut, setbacks, helical and so on. Dynamic wind-induced response analyses of these models have also been conducted. The results of these experiments have led to comprehensive understanding of the aerodynamic characteristics of tall buildings with various configurations.

Keywords: Tall building, Corner modification, Setback, Tapered building, Helical-shaped building, Building with openings, Combined configurations

1. Introduction

Since the completion of Burj Kalifa in 2010, some super-tall buildings over 1,000 m high have been planned. The current tallest building in the world is the 828 m-high Burj Khalifa, and the tallest building in the next decade will be Kingdom Tower (over 1000 m), which will be completed in 2018, making Burj Khalifa the third tallest. This trend of tall building construction, i.e., manhattanization, requires attention, particularly the preference for free-style building shapes rather than simple conventional building shapes, which are seen in Burj Kalifa and Shanghai Tower, presently under construction. These freewheeling building shapes have advantages not only in architectural design reflecting architects' challenging spirits for new forms but also in structural design reducing wind loads. In particular, across-wind response, which is a major factor in safety and habitability of tall buildings, is greatly suppressed.

The effectiveness of aerodynamic modification to reduce wind loads has been widely reported, and aerodynamic

modifications thought to be effective include those to sectional shape (horizontally) such as polygon or Y-type (Hayashida and Iwasa, 1990; Hayashida et al., 1992) and corners (Shiraishi et al., 1986; Kwok et al., 1988; Miyashita et al., 1993; Amano, 1995; Kawai, 1998), building shape (vertically) such as taper (Cooper et al., 1997; Kim and You, 2002; Kim et al., 2008; Kim and Kanda, 2011, 2013) and setback (Kim and Kanda, 2011, 2013), as well as introduction of openings (Dutton and Isyumou, 1990; Miyashita et al., 1993). However, most of the above papers have focused on the effect of one aerodynamic modification that changes systematically. For example, for corner-modification buildings, various modification shapes and various modification lengths were highlighted, and for tapered buildings, the effects of different taper ratios were the main concern. Although there have been some reports on cross comparisons of different aerodynamic modifications using a limited number of aerodynamic modifications, none have comprehensively investigated aerodynamic characteristics of various types of tall buildings with different configurations.

The purpose of the present study is to investigate the aerodynamic characteristics of tall buildings with unconventional building configurations to provide the structural designer with comprehensive wind tunnel test data that

[†]Corresponding author: Hideyuki Tanaka
Tel: +81-476-77-1352; Fax: +81-476-47-7333
E-mail: tanaka.hideyuki@takenaka.co.jp

can be used in the preliminary design stage. Aerodynamic forces on tall building models with the same volume were firstly measured, and then wind pressure measurements and CFD (Computational Fluid Dynamics) calculations were conducted for the models which showed excellent aerodynamic characteristics. After examining aerodynamic force characteristics, detailed response analyses were conducted and the efficiency of each building shape in terms of wind-resistant design was evaluated. The present paper expands on the report of Tanaka et al. (2012).

2. Outline of Wind Tunnel Experimental Models

2.1. Configuration of tall building models

The tall building models used for the experiments are shown in Tables 1(a)–(g). Following the previous study (Tanaka et al., 2012), discussions on 5 building models with triangular cross-sections were added. The full-scale height and the total volume of each building model are commonly set at $H = 400$ m (80 stories) and about $1,000,000\text{m}^3$. The width B of the Square Model shown in Table 1(a) is 50 m and the aspect ratio H/B is 8. The geometric scale of the wind tunnel models is set at $1/1000$. The tall building models examined in this study are classified in 7 categories as follows.

2.1.1. Basic models

The Square, Rectangular, Triangular, Circular, and Elliptic plan models shown in Table 1(a) are classified as Basic Models. The side ratio of the Rectangular and Elliptic Models is 1:2. For the Circular and Elliptic Models, the effect of Reynolds number Re should be discussed when considering the correspondence to the full-scale structure. Generally it is quite difficult to simulate a large Re which is similar to full-scale, so in the present work, Re is just mentioned as a reference for the smooth-surfaced models. The Re obtained from the diameter of the Circular Model used in the wind tunnel experiment is $Re = 2.9 \times 10^4$. The detail of Triangular plan Models is shown in previous report (Kumar et al., 2012).

2.1.2. Corner modification models

Although there are several methods for corner modification, i.e., corner chamfered, corner cut, corner rounding, fin, and so on, the examination of corner modification focuses on a Corner Cut Model, a Corner Chamfered Model and a Tri-Corner Cut Model as shown in Table 1(b). Referring to past researches on aerodynamic characteristics of structures and buildings with corner chamfered and corner cut models (Shiraishi et al., 1986; Amano, 1995; Kawai, 1998), the modification length is set at $0.1B$, where B is the building width.

2.1.3. Tilted models

For the Tilted Model, the roof floor is displaced by $2B$

from the base floor, and for the Winding Model, the floors at $0.25H$ and $0.75H$ are shifted by $0.5B$ to the left and right side, respectively, from the middle floor, and the walls have smoothly curved surfaces as shown in Table 1(c).

2.1.4. Tapered models

The tapered models include the following five types: a 2-Tapered Model which has only two tapered surfaces, a 4-Tapered Model which has four tapered surfaces, an Inversely 4-Tapered Model which has the inverse building shape of the 4-Tapered Model, and a Bulged Model whose sectional area at mid-height is expanded as shown in Table 1(d). When the taper ratio is between 5% and 10%, a model with a larger tapering ratio shows better aerodynamic behavior (Kim and Kanda, 2010a, 2010b). Thus, for the 4-Tapered Model, the taper ratio was set at 10% and the area ratio of the roof floor to the base floor was set at $1/6$. The Setback Model with a 4-layer setback is also classified in this category. The area ratio of the roof floor to the base floor is set at $1/6$ for the 2-Tapered, Setback, and Inversely 4-Tapered Models. For the Bulged Model, the ratio of roof floor or base floor area to the largest middle floor area is $1/3$.











2.1.5. Helical models

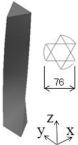
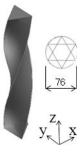
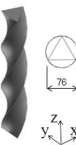



The sectional shapes of the helical models are square, rectangular and triangular, and the twist angle θ between the roof floor and the base floor is set at 60° , 90° , 180° , 270° and 360° , as shown in Table 1(e). The sectional shapes together with the twist angle are used as a prefix of the

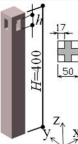
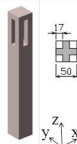
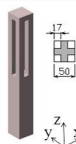
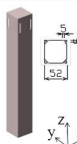
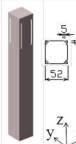
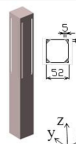






Table 1. Configuration of test models



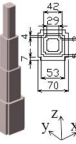
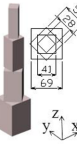




(a) Basic models				
Square	Rectangular	Triangular	Circular	Elliptic
(b) Corner modification models			(c) Tilted models	
Corner Chamfered	Corner Cut	Tri-Corner Cut	Tilted	Winding
(d) Tapered models				
2-Tapered	4-Tapered	Setback	Inversely 4-Tapered	Bulged

Table 1. Configuration of test models (continued)

(e) Helical models				
90° Helical Square	180° Helical Square	270° Helical Square	360° Helical Square	180° Helical Rectangular
				
				
Z_0 Y_0 X	Z_0 Y_0 X	Z_0 Y_0 X	Z_0 Y_0 X	Z_0 Y_0 X

(e) Helical models		
60° Helical Triangular	180° Helical Triangular	360° Helical Triangular
		
		
Z_0 Y_0 X	Z_0 Y_0 X	Z_0 Y_0 X

(f) Opening models					
(f-1) Cross Opening			(f-2) Oblique Opening		
$h/H=2/24$	$h/H=5/24$	$h/H=11/24$	$h/H=2/24$	$h/H=5/24$	$h/H=11/24$
					
					
Z_0 Y_0 X	Z_0 Y_0 X	Z_0 Y_0 X	Z_0 Y_0 X	Z_0 Y_0 X	Z_0 Y_0 X

(g) Composite models			
360° Helical & Corner Cut	4-Tapered & 360° Helical & Corner Cut	Setback & Corner Cut	Setback & 45° Rotate
			
			
Z_0 Y_0 X	Z_0 Y_0 X	Z_0 Y_0 X	Z_0 Y_0 X

Notes: Category (b)–(f) are single modification models and (g) is multiple modifications model.

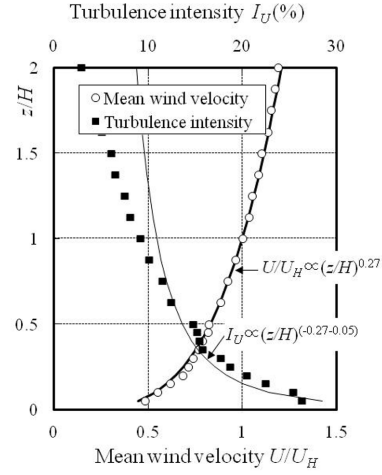
model name. For example, the 180° Helical Square Model means the helical model whose sectional shape is square with a twist angle of 180°.

2.1.6. Opening models

In the category of opening models, three cross opening models and three oblique opening models, whose openings are provided at the top-center and top-corner of the walls, respectively, are classified as shown in Table 1(f). Three different opening heights $h = 2H/24$, $5H/24$, and $11H/24$ are considered to clarify the effects of opening size on the aerodynamic characteristics. For the three Oblique Opening Models, the opening volume is not included in the building volume, and since the building volumes of those Models is almost the same, their widths are fixed. However, for the three Cross Opening Models, the opening volume is included in the building volume, because of the compatibility of aspect ratio with the other models.

2.1.7. Composite models

The composite models have the combined configurations

**Figure 1.** Flow conditions of wind tunnel experiment.

of the primary configurations shown in Tables 1(a)–(f), and the aerodynamic characteristics of the following four composite models shown in Table 1(g) are investigated: 360° Helical & Corner Cut Model; 4-Tapered & 360° Helical & Corner Cut Model; Setback & Corner Cut Model; and 45° Rotating Setback Model, where the rotating angle of each setback layer is 45°.

2.2 Experimental condition

2.2.1. Aerodynamic force measurements

Wind tunnel experiments were performed in a closed-circuit-type boundary-layer wind tunnel whose working section is 1.8 m high by 2.0 m wide. Figure 1 shows the condition of the approaching turbulent boundary layer flow with a power-law index of 0.27, representing an urban area. The wind velocity and turbulence intensity at the top of the model are about $U_H = 7.0$ m/s and $I_{UH} = 9.2\%$, respectively. The turbulence scale near the model top is about 0.360 m, and that of AIJ-RLB (AIJ, 2004a) is 365 m. Therefore, when considering the length scale of 1/1000, the flow conditions of the present work are thought to be appropriately simulated. The detail of wind tunnel experiment for Triangular plan Models is shown in the report of Kumar et al. (2012). Dynamic wind forces were measured by a 6-component high-frequency force balance (HFFB) supporting light-weight and stiff models. Wind direction α is changed from 0°, which is normal to a wall surface, to 45° or 180° every 5° depending upon the building configuration. The measured wind forces and aerodynamic moments are normalized by $q_H B H^2$ to get wind force coefficients and moment coefficients. Here, q_H is the velocity pressure at the model height H , and B is commonly set at the width of the Square Model. Therefore, the force and moment coefficients of the models can be directly compared. Figure 2 shows the definitions of wind forces, moments, and the coordinate system employed in this study. The Reynolds number R_e based on the mean wind velocity at the roof height U_H and the width of the Square

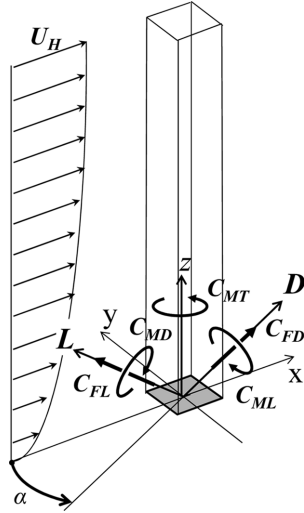


Figure 2. Coordinate system.

Model *B* is $Re = 2.6 \times 10^4$.

2.2.2. Wind pressure measurements

Wind pressure measurements were conducted on 12 models. They were determined from the results of aerodynamic force measurements and for relatively realistic building shapes in the current era. The aims of the pressure measurement were to examine the characteristics of local wind forces and aerodynamic phenomena in detail. In addition, the wind response analysis was conducted using a result of the pressure measurement.

The coordinate system and approaching flow for the wind pressure measurements are the same as for the aerodynamic force measurement (see Figs. 1 and 2), except

that the wind velocity at model height was 11.8 m/s. Also, the wind direction was changed from 0° to 355° at 5° intervals as for the aerodynamic force measurements. The fluctuating wind pressures of each pressure tap were measured and recorded simultaneously using a vinyl tube 80 cm long through a synchronous multi-pressure sensing system (SMPSS). The sampling frequency was 1 kHz with a low-pass filter of 500 Hz. The total number of data was 32,768. The fluctuating wind pressures were revised considering the transfer function of the vinyl tube.

There were about 20 measurement points on one level on four surfaces, and the measurement points were instrumented at 10 levels (12 levels only for Setback Model), giving about 200 measurement points. The wind pressure coefficients C_p were obtained by normalizing the fluctuating pressures p by the velocity pressure q_H at model height. The local wind force coefficients, C_{FD} for along-wind, C_{FL} for across-wind and C_{mT} for torsional moment, were derived by integrating the wind pressure coefficients C_p using the building width of the Square Model *B* (B^2 for torsional moment) regardless of building shape.

3. Outline of Numerical Simulation

3.1. Large-eddy simulation

Table 2 shows the outlines of numerical simulations. For the SGS model in LES (Large-Eddy Simulation), the standard Smagorinsky model with $C_s = 0.12$ was used. The approaching flow was simulated in the driver domain (Fig. 3(a)) in the same way as in the wind tunnel, and the numerical calculations were conducted in the simulation domain (Fig. 3(b)) using the approaching flow as the inflow boundary condition. Four building models including Squa-

Table 2. Outlines of numerical simulation

Coordinate system	Cartesian coordinates	
Grid system	Non-uniform staggered grid system (Kajishima, 1999)	
Algorism	SMAC method	
Velocity prediction	PSOR2 method	
Poisson solver	Residual cutting method (Tamura et al., 1997) using Bi-CGSTAB method for inner solver	
Spatial difference scheme	Combined use of 2nd and 4th order centered difference scheme (Morinishi et al., 1998)	
Time scheme	Convective terms & Eddy viscosity terms : 3rd order Adams-Bashforth method Molecular viscosity terms : Crank- Nicolson method	

Table 3. Conditions of numerical simulation

Computational domain	Driver domain	$270B(x) \times 40B(y) \times 36B(z)$
	Simulation domain	$49B(x) \times 25B(y) \times 24B(z)$
Grid discretization	Driver domain	$1504(x) \times 340(y) \times 72(z) = 36,817,920$
	Simulation domain	$256(x) \times 240(y) \times 272(z) = 16,711,680$
Grid size adjacent to building wall surface		0.01 <i>B</i>
Inflow boundary	Driver domain	Uniform flow
	Simulation domain	Inflow turbulence generated in the driver domain
Downstream boundary		Convective boundary condition
Lateral and upper surfaces of computational domain		Zero gradient condition
Ground surface and Building surface boundary		Two Layer Model (Werner and Wengel, 1991)

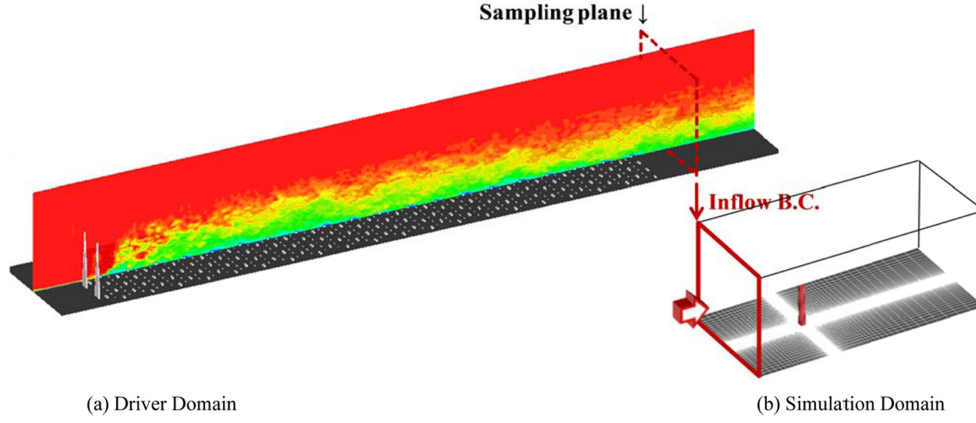


Figure 3. Driver and Simulation domain.

re, Corner Cut, Setback, and 180° Helical Square were used in the simulation, and the details of numerical simulations are shown in Table 3.

The approaching flow in the driver domain was simulated by modeling the spires and roughness blocks as shown in Fig. 3(a), and Fig. 4 shows the vertical profiles of the mean component U/U_H and the turbulence intensity I of the simulated approaching flow used as inflow boundary condition. The power spectrum of the fluctuating component U_H' at building height is shown in Fig. 4(c). In the numerical simulations, the intervals of the normalized time difference were $tU_H/B = 2.0 \times 10^{-3}$, and the results of 10-minute full scale data corresponding to the normalized time differencing $tU_H/B = 850$ are shown. The Reynolds number of the numerical simulation was $Re = 3.9 \times 10^4$.

3.2. Accuracy of in-house code for Large-eddy simulation

Cross-comparisons of mean and fluctuating pressure coefficients of Square, Corner Cut, Setback, and 180° Helical Square are shown in Fig. 5. LES results were interpolated considering the pressure tap positions. For 180° Helical Square, as the building shape is quite complicated, it

was approximated by the Voxel method. The correspondence to the pressure measurement results was inferior to those of other building shapes. However, as the grid size near the building surfaces was small enough, the agreements with the pressure measurement results are generally good, implying the high quality of the in-house code for LES. This also means that high quality is ensured in the reproduction of wind flows around buildings discussed later.

4. Results of Wind Force Measurements

4.1. Overturning moment coefficients

Figure 6 shows the variation of the mean along-wind overturning moment (o.t.m.) coefficient $\overline{C_{MD}}$ and the mean across-wind o.t.m. coefficient $\overline{C_{ML}}$ with wind direction α for the test models which show specific aerodynamic force characteristics. And, the comparisons of HFFB results with those of SMPSS are shown in Fig. 6, showing good agreement between them. The maximum values of $\overline{C_{MD}}$ and $\overline{C_{ML}}$ considering all wind directions are defined as the maximum along-wind and across-wind mean o.t.m. coefficients $|\overline{C_{MD}}|_{\max}$ and $|\overline{C_{ML}}|_{\max}$. The maximum values of C_{MD}'

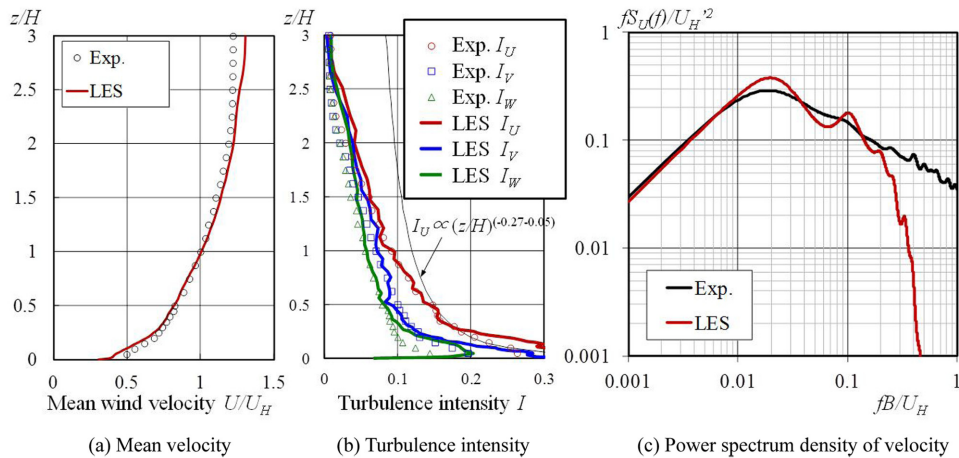


Figure 4. Inflow boundary condition for LES.

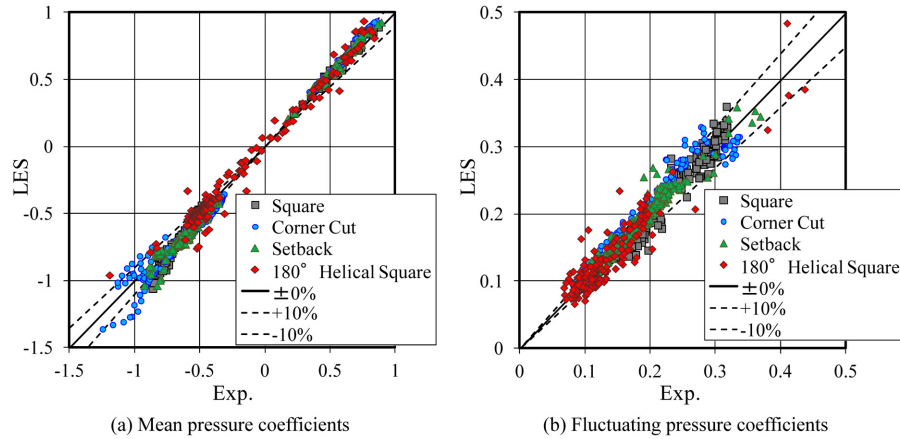


Figure 5. Cross-comparison for pressure coefficients.

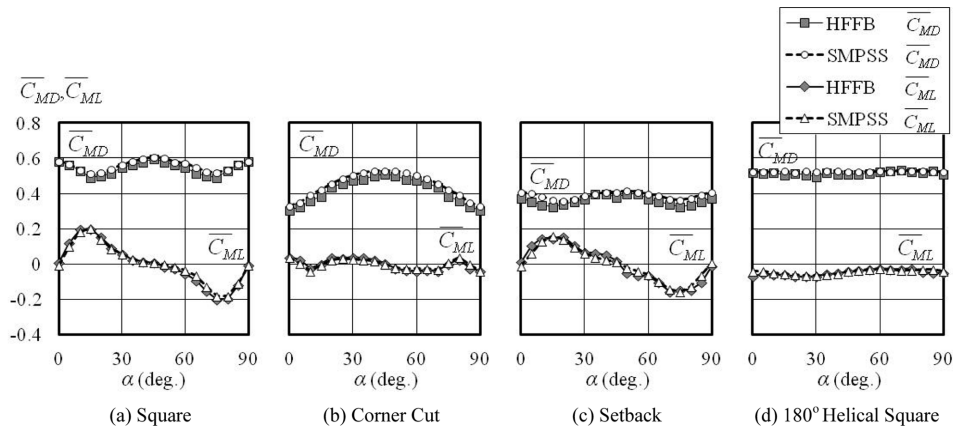


Figure 6. Variation of mean overturning moment coefficients on wind direction for some test models.

and C_{ML}' considering all wind directions are similarly defined as the maximum along-wind and across-wind fluctuating o.t.m. coefficients $C_{MD}'_{max}$ and $C_{ML}'_{max}$. The coefficients C_{MD}' and C_{ML}' are the standard deviation of the o.t.m. These variation of $|C_{MD}'|_{max}$, $|C_{ML}'|_{max}$, $C_{MD}'_{max}$ and $C_{ML}'_{max}$ for the building configurations are discussed below.

4.1.1. Mean overturning moment coefficients

Figure 7 shows the maximum values of the mean along-wind and across-wind o.t.m. coefficients, $|C_{MD}'|_{max}$ and $|C_{ML}'|_{max}$ considering all wind directions. The maximum mean along-wind o.t.m. coefficients $|C_{MD}'|_{max}$ of the 4-Tapered Model and the Setback Model, whose sectional area decreases with height, are relatively small. The maximum mean across-wind o.t.m. coefficients $|C_{ML}'|_{max}$ of the Corner Cut Model and Corner Chamfered Model are small. The maximum mean across-wind o.t.m. coefficients of the Helical Square Model and the Cross Opening $h/H = 11/24$ Model, whose opening size is the largest, are also small. The maximum mean o.t.m. coefficients $|C_{MD}'|_{max}$ and $|C_{ML}'|_{max}$ of a Helical Square/Triangular Model with a larger twist angle tends to show smaller values. And, as can be seen in Fig. 6, the variations of mean o.t.m. coeffi-

cients $\overline{C_{MD}}$ and $\overline{C_{ML}}$ of the 180°Helical Square Models with wind direction are very small. The maximum mean o.t.m. coefficients $|C_{MD}'|_{max}$ and $|C_{ML}'|_{max}$ of Rectangular cross-section Models (Rectangular Model and 180°Helical Rectangular Model) and Triangular cross-section Models (Triangular Model, Tri-Corner Cut Models and Helical Triangular Models) are larger than those of the Square cross-section Models. The aerodynamic characteristics of the composite models with multiple modifications are mostly superior to those of the models with single modification.

4.1.2. Fluctuating overturning moment coefficients

Figure 8 shows the maximum along-wind and across-wind fluctuating o.t.m. coefficients, $C_{MD}'_{max}$ and $C_{ML}'_{max}$, considering all wind directions. As shown in Fig. 8, the maximum fluctuating along-wind o.t.m. coefficients $C_{MD}'_{max}$ of the Corner Chamfered, Corner Cut, 4-Tapered and Setback Models are smaller. The maximum fluctuating across-wind o.t.m. coefficients $C_{ML}'_{max}$ of the 4-Tapered, Setback, Helical Square, and Cross Opening 11/24 Models show relatively small values. These trends are the same as those of the maximum mean o.t.m. coefficients. And, the effect of twist angle θ for the Helical Square/

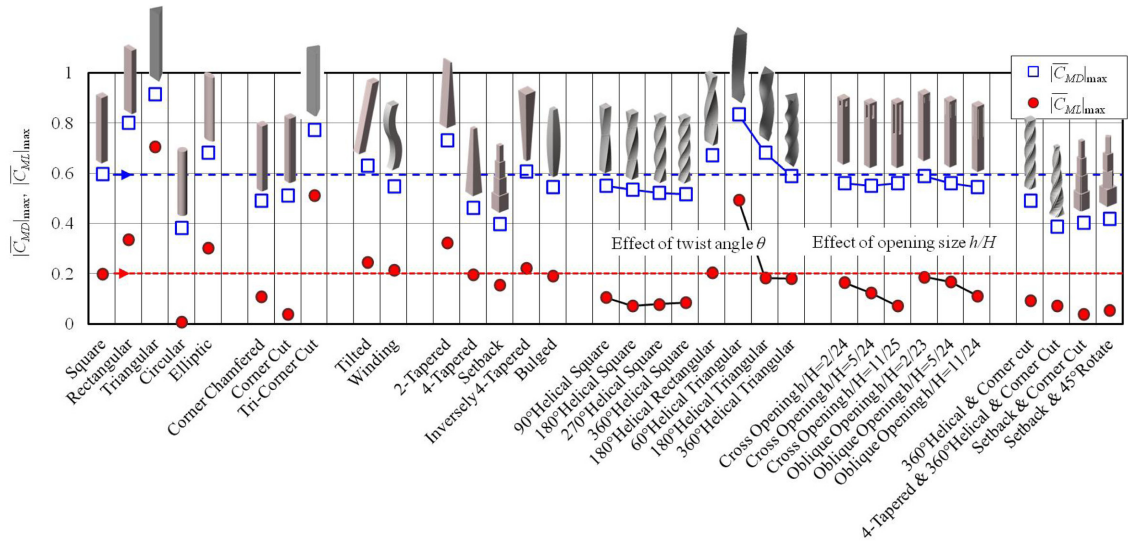


Figure 7. Comparison of maximum mean overturning moment coefficients.

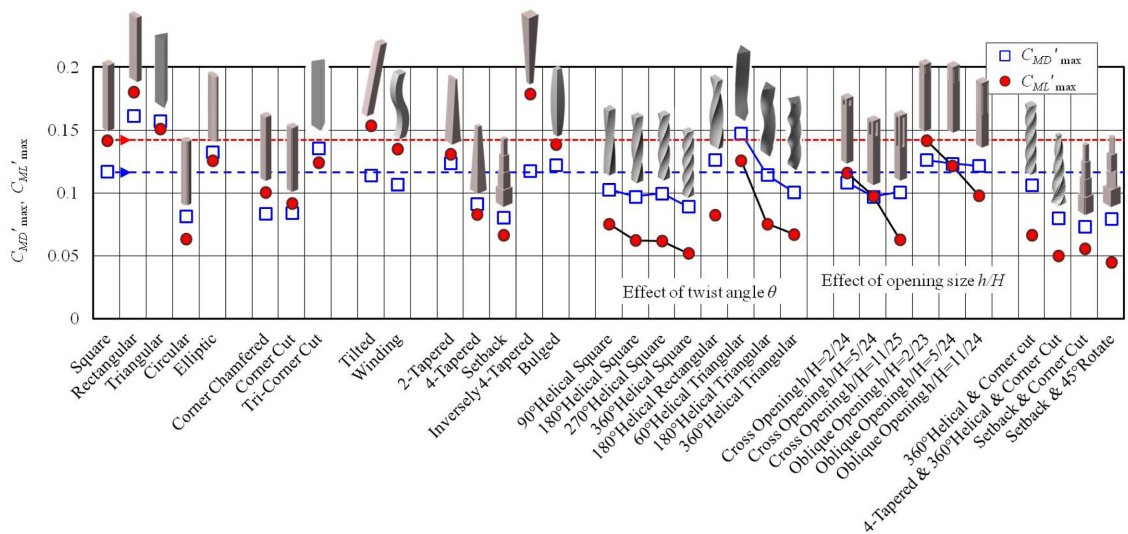


Figure 8. Comparison of maximum fluctuating overturning moment coefficients.

Triangular Models, the effects of opening size for the two types of Opening Models, and the composite effect also show the same tendency as those of the maximum mean o.t.m. coefficients. Because the effects of twist angle θ on the fluctuating across-wind o.t.m. $C'_{ML,max}$ are large, detailed comparisons of fluctuating across-wind o.t.m. $C'_{ML,max}$ are shown in Fig. 9. Fluctuating across-wind o.t.m. $C'_{ML,max}$ in Fig. 9 are shown as the ratio to that of the Basic Models of same cross-section. The maximum fluctuating across-wind o.t.m. $C'_{ML,max}$ becomes a half of that of the Basic Model when the twist angle is larger than 180° .

4.1.3. Relationship between overturning moment coefficients

The relationship between maximum mean o.t.m. coefficients and maximum fluctuating o.t.m. coefficients for all

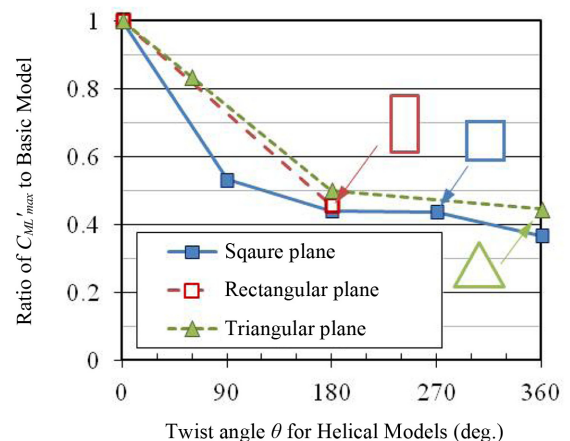


Figure 9. Effect of twist angle θ for Helical Models.

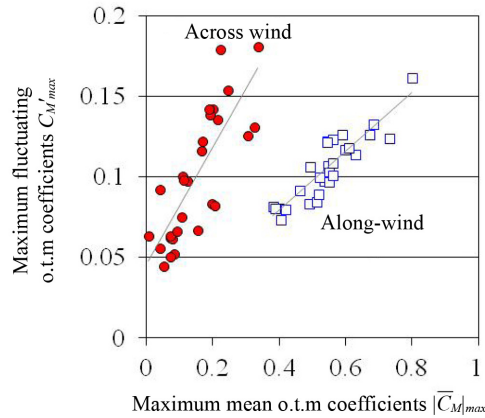


Figure 10. Relationship between maximum mean and maximum fluctuating o.t.m. coefficients.

building models are shown in Fig. 10 for the along-wind direction and for the across-wind direction. Figure 11 shows the relationship between the maximum mean o.t.m. coefficients in the along-wind direction and those in the across-wind direction (Fig. 11(a)), and the relationship between the maximum fluctuating o.t.m. coefficients in both directions (Fig. 11(b)). As described in section 3.1.2., the maximum mean and fluctuating o.t.m. coefficients show a similar tendency, and high correlations between them are observed as shown in Fig. 10. And, it is interesting to note that the high correlations between mean/fluctuating o.t.m. coefficients in the along-wind direction and in the across-wind direction are observed.

5. Results of Wind-induced Responses Analysis

5.1. Analysis models

The wind pressure measurements were carried out on 12 models, including 8 single-modification models and 4 composite-modification models. The single-modification models include: Square Model, Corner Chamfered Model,

Corner Cut Model, 4-Tapered Model, Setback Model, two Helical Models ($\theta = 90^\circ$ and 180°), and Cross Opening Model ($h/H = 5/24$). The composite-modification models include: 180° Helical & Corner Cut Model, 4-Tapered & 180° Helical Model, and two 4-Tapered & Helical ($\theta = 180^\circ$ and 360°) & Corner Cut Models. Response analyses were conducted for these 12 models. Modeling of analysis models for response analyses were conducted as follows.

Step 1: Modeling the frame of a Square Model of an 80-story building whose building density is $170\sim 190 \text{ kg/m}^2$. The structural system was assumed to have a center core with a truss floor every 20 stories.

Step 2: For the frame model in Step 1, static analysis was conducted. Based on the analysis results, the shell model of the Square Model which consists of a bending-shear spring at the core and exterior shell elements was made such that its static analysis results were the same as those of the frame model.

Step 3: Without changing the characteristics of the bending-shear spring and exterior shell elements of the Square model, only the shapes of the exterior shell elements were changed considering the building shapes.

The results of the eigenvalue analysis for the shell models are shown in Fig. 12 and Table 4 (for details, see Tamura et al., 2011). The eigenvalue analysis results showed that there were large differences between the 4-Tapered and Setback models and other models.

5.2. Evaluation of wind load

Response analyses were conducted for the design wind speed at the building top ranging from 30 m/s to 71 m/s at 1 m/s intervals. Here, 71 m/s corresponds to the 500-year-return-period design wind speed. The response analyses were conducted from 0° to 90° at 5° intervals (total of 19 wind directions) for two translational and a torsional direction. For the two translational directions, the first four modes were considered, and for the torsional direction, the first three modes were considered. The responses of each mode were obtained from the spectral model

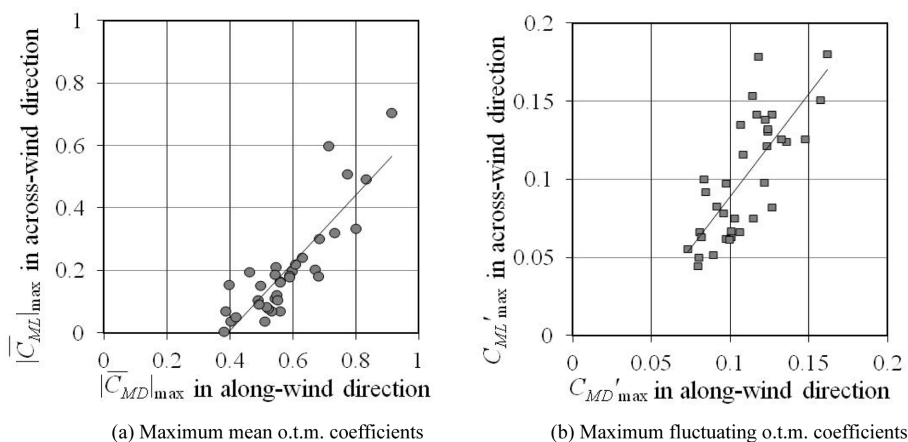


Figure 11. Relationship between along-wind direction and across-wind direction.

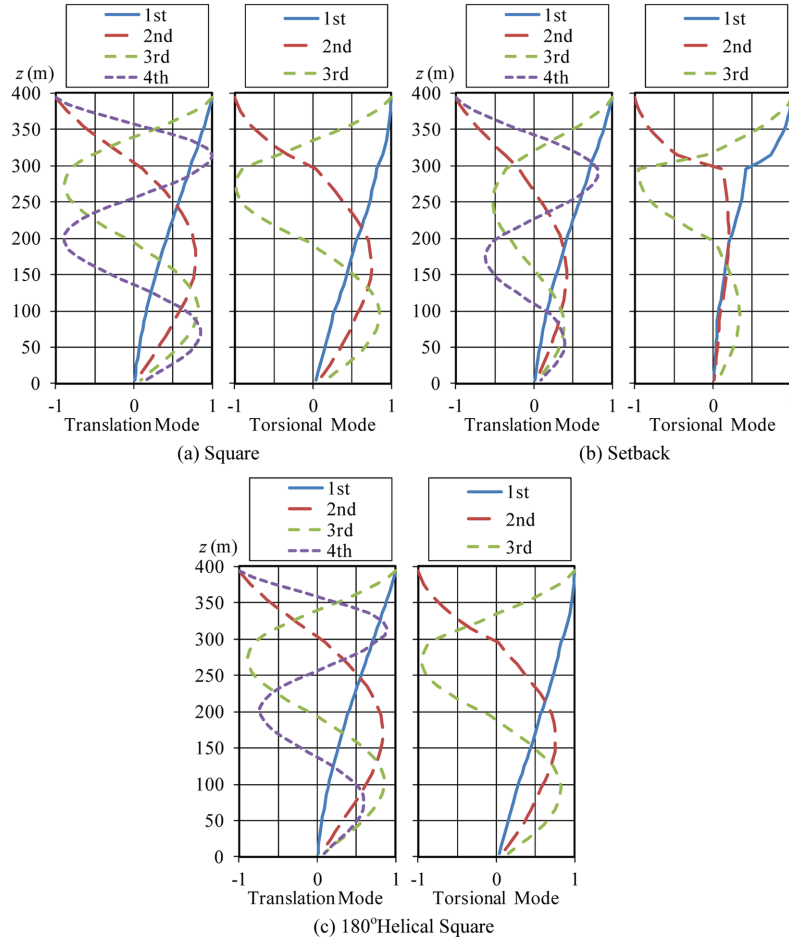


Figure 12. Natural vibration mode.

Table 4. Natural frequency of response analysis models

Model	Translation (Hz)				Torsion (Hz)		
	1st	2nd	3rd	4th	1st	2nd	3rd
Square	0.096	0.312	0.578	0.838	0.178	0.462	0.761
Cross Opening ^{*1}	0.110	0.315	0.559	0.863	0.201	0.481	0.752
Corner Chamfered ^{*2}	0.096	0.312	0.578	0.838	0.178	0.462	0.761
Corner Cut ^{*2}	0.096	0.312	0.578	0.838	0.178	0.462	0.761
4-Tapered	0.150	0.353	0.614	0.874	0.300	0.529	0.800
Setback	0.157	0.363	0.608	0.856	0.310	0.452	0.685
90° Helical Square	0.093	0.312	0.580	0.845	0.183	0.475	0.780
180° Helical Square	0.092	0.312	0.581	0.854	0.188	0.493	0.812
180° Helical & Corner Cut ^{*3}	0.092	0.312	0.581	0.854	0.188	0.493	0.812
4-Tapered & 180° Helical ^{*4}	0.150	0.353	0.614	0.874	0.300	0.529	0.800
4-Tapered & 180° Helical & Corner Cut ^{*4}	0.150	0.353	0.614	0.874	0.300	0.529	0.800
4-Tapered & 360° Helical & Corner Cut ^{*4}	0.150	0.353	0.614	0.874	0.300	0.529	0.800

^{*1} To model the center core up to the top of the building, the cross opening was divided into two parts which are located at both edges.

^{*2} The dynamic characteristics of the Corner Chamfered Model and Corner Cut Model were assumed to be the same as that of the Square Model.

^{*3} The dynamic characteristics of 180° Helical & Corner Cut was assumed to be the same as that of the 180° Helical Model.

^{*4} For the composite model of 4-Tapered Model with helical and corner cut, the dynamic characteristics were assumed to be the same as the 4-Tapered Model.

method, and the total responses were calculated using the root mean square of each mode. A damping ratio of 2%

for each mode was considered, and the peak factor g_j of the j^{th} mode was calculated from Eq. (1) using the natural

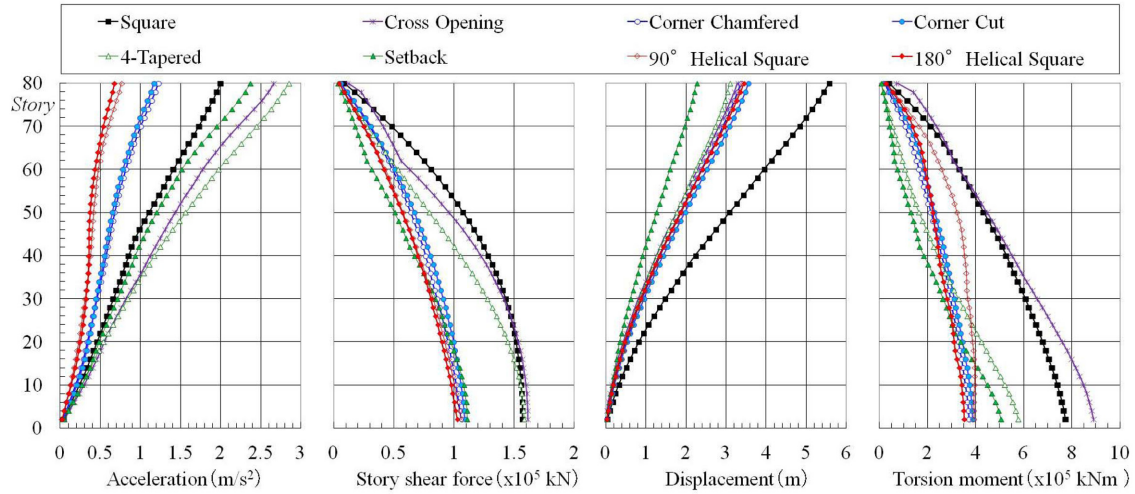


Figure 13. Vertical profile of wind-induced responses with single modification for 500-year return period design wind speed.

frequency n_j .

$$g_j = \sqrt{2 \ln(600n_j) + 1.2} \quad (1)$$

For the shear force and torsional moment of each floor, the mean components were calculated by summing the mean external forces of upstairs, and the fluctuating components were also calculated by summing the external forces of upstairs obtained from the accelerations acting on each mass beforehand. Here, in order to also consider the long-period component of acceleration, $(2\pi n)^2$ was multiplied by the fluctuating displacement and torsional angle in the first mode. And the mean displacement \bar{y} was obtained from the mean overturning moment \bar{M} , the fluctuating overturning moment $\sigma_{M,j}$, and fluctuating displacement $\sigma_{y,j}$, as shown in Eq. (2).

$$\bar{y} = \frac{\sqrt{\sum_j (g_j \sigma_{y,j})^2} \times \bar{M}}{\sqrt{\sum_j (g_j \sigma_{M,j})^2}} \quad (2)$$

Figure 13 shows the vertical profiles of the accelerations, story shear forces, displacements, and torsional moments of 8 single-modification models. The values in Fig. 13 are the largest values for all wind directions within the design wind speed ranges. The accelerations of the Corner modification Models and Helical models are greatly reduced compared with that of the Square Model, having higher mode effects. The story shear forces of the Corner modification Models, Setback Model, and Helical models are also reduced compared to that of the Square Model, but does not show higher mode effects. For displacements, there are no higher model effects, and the displacements of all models show smaller values than that of the Square Model. For the torsional moments, the effect of twist angle is clearly seen, i.e., the larger torsional moment at upper height becomes smaller when changing the twist angle from 90° to 180°.

The maximum acceleration, maximum story shear coefficient

cient, maximum displacement, maximum story deformation angle, maximum story shear force, maximum overturning moment, and maximum torsional moment of all models are shown in Fig. 14. All maximum values in Fig. 14 are shown as the ratio to that of the Square model. The single modification models that show smaller responses for all items are Corner Cut, Corner Chamfered, 90°Helical and 180°Helical. For the 4-Tapered, Setback, Cross Opening, the maximum acceleration and the maximum story shear coefficient are larger than that of the Square Model. All composite models show smaller values for all items. When comparing the 4-Tapered & 180°Helical Model with the 4-Tapered Model with the same structural characteristics, the suppression of response is significant. For the 180° Helical & Corner Cut Model and 4-Tapered & Helical & Corner Cut Model, only the maximum torsional moment is suppressed. For two composite models with different helical angles of 4-Tapered & 180°Helical & Corner Cut

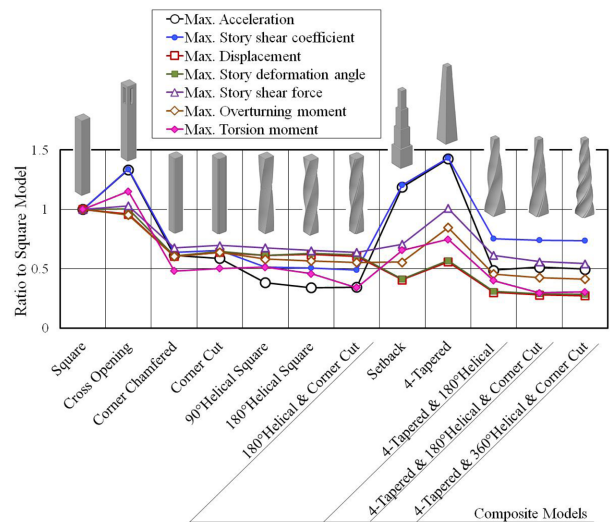


Figure 14. Comparison of wind-induced responses for 500-year return period design wind speed.

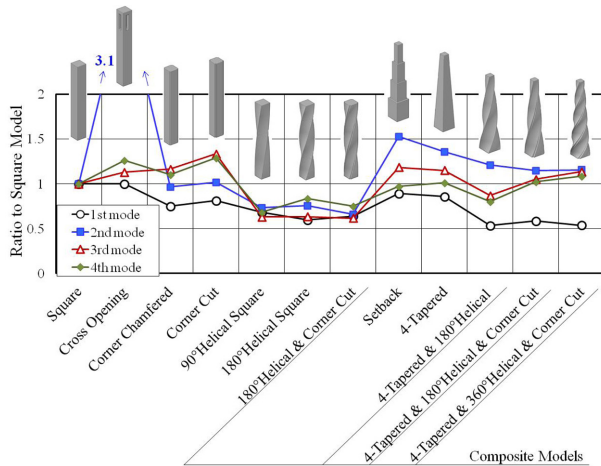


Figure 15. Comparison of accelerations for 1-year return period design wind speed.

Model and 4-Tapered & 360° Helical & Corner Cut Model, there is little difference for all items, implying that the helical angle of 180° is enough.

5.3. Evaluation of habitability

The analysis models for habitability are the same as the models in section 5.2., but the dynamic characteristics were changed slightly to consider the effects of secondary members; the natural frequencies were assumed to be 20% higher, and the damping ratios were assumed to be 0.7%. The design wind speed for habitability is 31 m/s. The analytical procedures are the same as in section 5.2., but as the sensitivity of the human body to vibration depends on the natural frequencies and corresponding accelerations, the acceleration responses of the 1st~4th modes were not superimposed.

Figure 15 compares the maximum accelerations of from the 1st to 4th modes for all wind directions. All maximum accelerations in Fig. 15 are shown as the ratio to that of the Square model. Of the single modification models, the 90° Helical and 180° Helical Models show smaller maximum

acceleration, showing better habitability. The first mode acceleration of the Corner Cut and Corner Chamfered Model is smaller than that of the Square Model, but those of the third and fourth modes are larger than that of the Square Model. The habitability of the 4-Tapered, Setback, Cross Opening Models is worse than that of the Square Model. In particular, the second mode acceleration of the Cross Opening Model is significantly larger, and this is because the second mode shape is similar to the vertical distribution of shear force. For composite models, the 180° Helical & Corner Cut shows smaller maximum accelerations, and the 4-Tapered & 180° Helical Model shows smaller maximum accelerations than the 4-Tapered Model, but when corner cut is combined (4-Tapered & 180° Helical Model & Corner Cut), the third and fourth maximum accelerations becomes larger.

Figure 16 compares the annual maximum accelerations with the guideline for the evaluation of habitability to building vibration prescribed in AIJ-RLB (2004b). The number on the right side of the graph indicates the ratio of the occupants who feel the vibration, i.e., H-30 means 30% of the occupants feel the vibration. Although the first mode maximum accelerations of the 90° Helical, 180° Helical, and 180° Helical & Corner Cut are larger than H-90, which is true for all other models, those of the second and third modes are smaller than H-50, and those of fourth mode are smaller than H-70 (Fig. 16(b)).

6. Discussions on Flow Characteristics Around Buildings

6.1. Power spectral density of across-wind local wind force coefficients

Although the wind tunnel tests were carried out on 33 models, only the 4 models with single modification will be discussed in this section: Square Model, Corner Cut Model, Setback Model and 180° Helical Models. The representative wind direction is $\alpha = 0^\circ$.

The power spectra of the across-wind local wind force

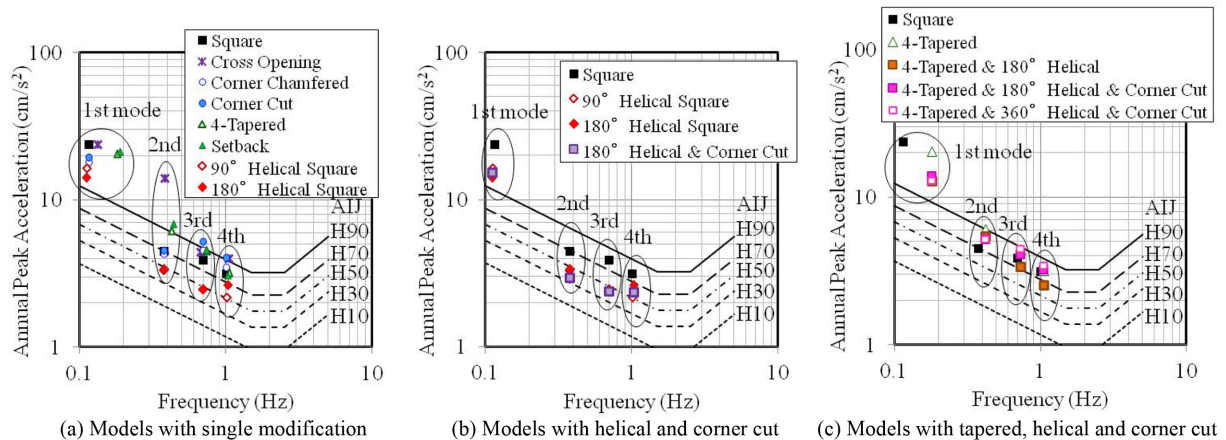


Figure 16. Annual maximum accelerations for habitability evaluation.

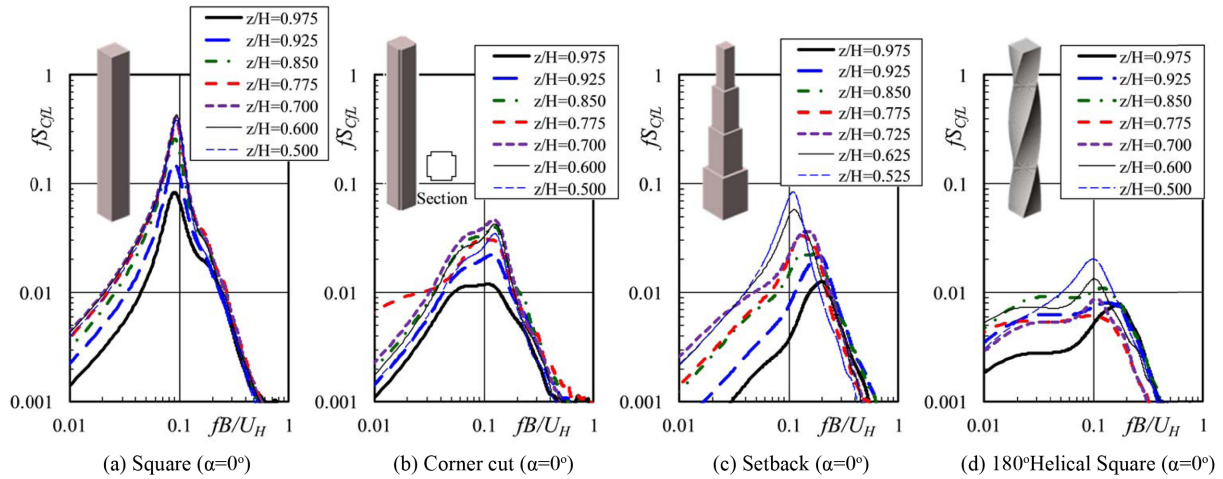


Figure 17. Power spectral densities of across-wind local wind force coefficients.

coefficient $fS_{C/L}$ higher than $z/H = 0.5$ are shown in Fig. 17. The Strouhal number S_t corresponding to the vortex shedding frequency, and the bandwidth B_w were obtained and the vertical profiles are shown in Figs. 18 and 19. The power spectra in Fig. 17 were plotted against the reduced frequency, which was obtained by using the width of the Square Model B (constant) regardless of building shape. The bandwidths B_w were obtained by approximating the power spectra $fS_{C/L}$ to Eq. (3) through the least-square method (Vickery and Clark, 1972).

$$\frac{fS_{C/L}}{\sigma^2} = k \frac{f}{\sqrt{\pi} f_{peak} B_w} \exp \left[- \left(\frac{1 - f/f_{peak}}{B_w} \right)^2 \right] \quad (3)$$

Sharp peaks near $z/H = 0.5$ were observed for the Square Model (Fig. 17(a)), but they become relatively flat near the model top because of the three-dimensional effect of flow. This again implies that regular vortex shedding exists near $z/H = 0.5$ and the regularity collapses near the model top, and the bandwidth shown in Fig. 19 near the $z/H = 0.5$ is smaller than that of the model top. The power spectral densities of other models in Figs. 17(b)–(d) show similar results.

The Strouhal numbers S_t of the Square Model and Cor-

ner Cut Model shown in Fig. 18 vary little with height, showing almost constant values throughout the height. This means that all the vortex components are shed almost the same time throughout the height. However, the Strouhal numbers of the Setback Model and 180° Helical Model vary greatly with height, implying that the shedding frequencies at each height are different.

Similar discussion can be made for the bandwidth shown in Fig. 19, i.e., regular and strong vortices with narrow-band are shed throughout the height for the Square Model, but for the other models, vortices with wide band are shed randomly.

6.2. Visualization of vortex shedding around buildings

To visualize the conditions of vortex shedding around buildings discussed in Section 6.1., the instantaneous iso-surfaces of pressure coefficients are shown in Figs. 19 and 20. Figure 20 shows the isosurface of pressure coefficients of -0.7, which demonstrates the 3-dimensional vortex structure. Figure 21 shows horizontal distributions of instantaneous pressure coefficients at two heights.

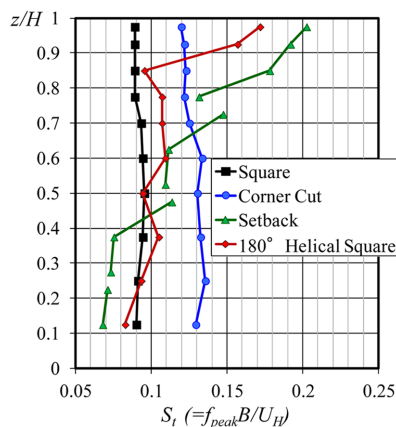


Figure 18. Vertical profile of Strouhal number.

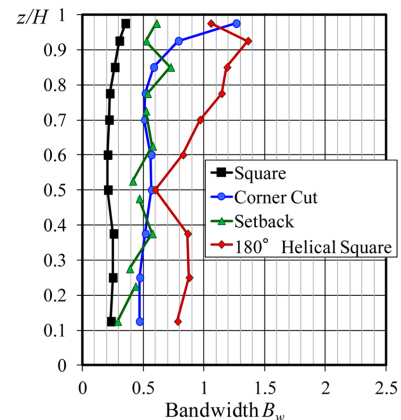


Figure 19. Vertical profile of bandwidth of across-wind local wind force power spectra.

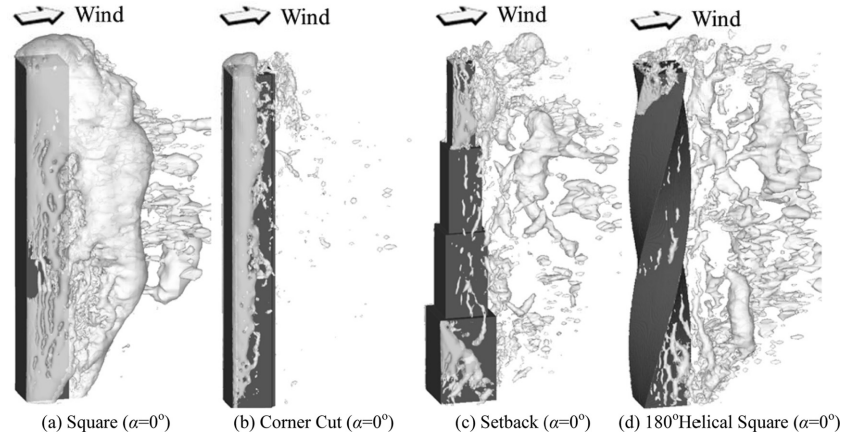


Figure 20. Visualization of instantaneous vortex structures around buildings (Isosurface of pressure coefficient $C_p = 0.7$).

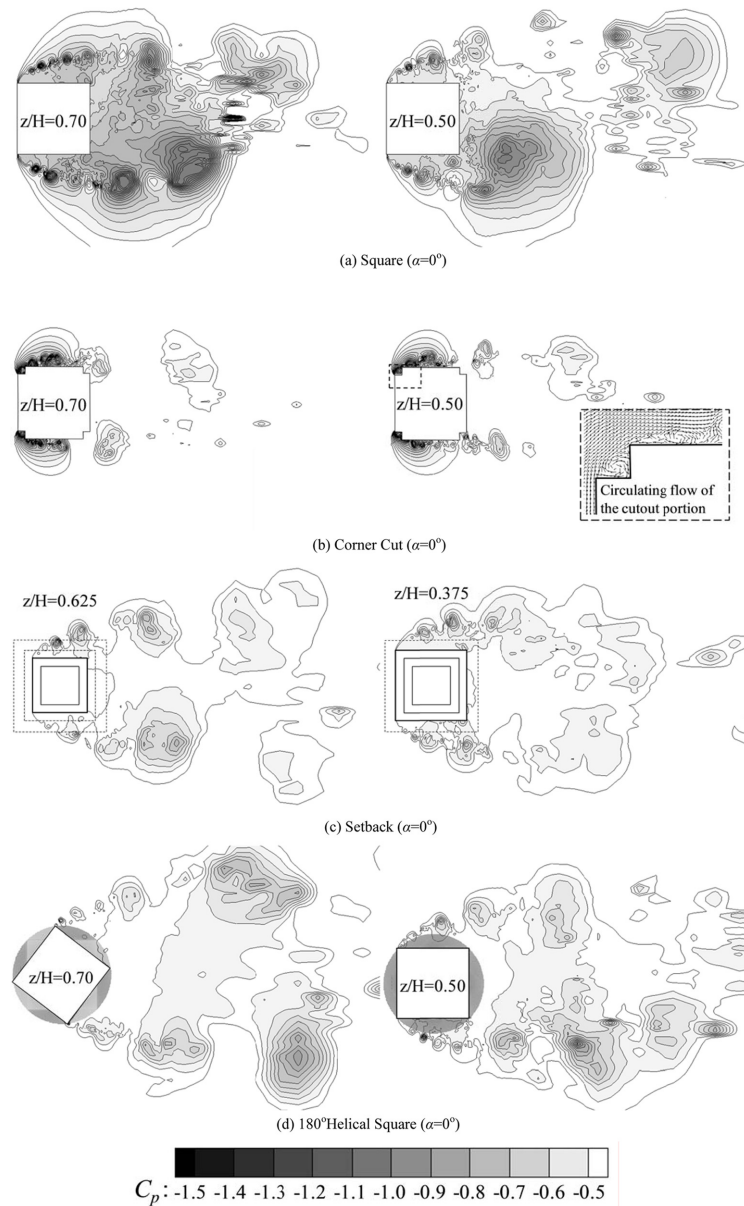


Figure 21. Horizontal distributions of instantaneous pressure coefficient.

For Square Model, large negative-pressure regions resulting from the periodic Karman vortex shedding were formed in the wake, as shown in Fig. 21(a). These regions were observed throughout most of the building height, as shown in Fig. 20(a). Because of this periodic and well-correlated Karman vortex shedding, a large across-wind force was applied to the Square Model. For the Corner Cut Model, although uniform vortex structures were found in the spanwise direction as for the Square Model (Fig. 20(b)), large negative-pressure regions were only found near the leading edges. This is because the circulation flows near the corner cut regions at the leading edges approximate the separated shear layers to the building side surfaces, disturbing the periodic vortex shedding, as shown in Fig. 21(b). For Setback Model and 180°Helical Square Model whose building shapes are modified in the spanwise direction, the vortex structures are significantly different from that of Square Model (Figs. 21(c) and (d)). The vortices shed in the wake are quite small, and vortex components at each height are shed at different time intervals (Figs. 20 (c) and (d)), resulting in smaller across-wind forces. When considering dimensions of B_w , vertical variations of S_f and peak power spectral values of local wind forces all together, the randomness or irregularity of vortex shedding is more profound in 180° Helical Square Model than in Setback Model.

For the Corner Cut Model, Setback Model and 180°Helical Square Model, as the vortex is formed in a position further from the building's leeward surface, the leeward pressures increase (absolute values decrease), resulting in a decrease in along-wind force. Thus, the mitigations of vortex shedding are effective for suppression of not only across-wind force but also of along-wind force. Considering this result, the high correlations between along- and across-wind forces, which are shown in Fig. 11, were well understood.

6.3. Effect of helical-shape on flow characteristics around buildings

In this section, for 180°Helical Square Model, the reason for the mitigation of vortex shedding and further position of vortex formation from the leeward surface is considered.

Figures 21 and 22 show the mean vertical flow conditions W/U_H near the building surface and around the building surface, respectively. As shown in Fig. 22, the mean vertical flows at the side surface are almost zero except building top for Square Model. For 180°Helical Model, however, the mean vertical flows near $z/H = 1.0, 0.5, 0.0$ are large, and there are flows along the building surfaces in the direction of the arrow as shown in Fig. 22(b). These flows along the building surfaces for 180°Helical Square Model occurred possibly because the positive and negative pressures are mixed on the same surface, as shown in Fig. 23. The flow conditions around buildings shown in Fig. 23 are also affected by these vertical flows, and the com-

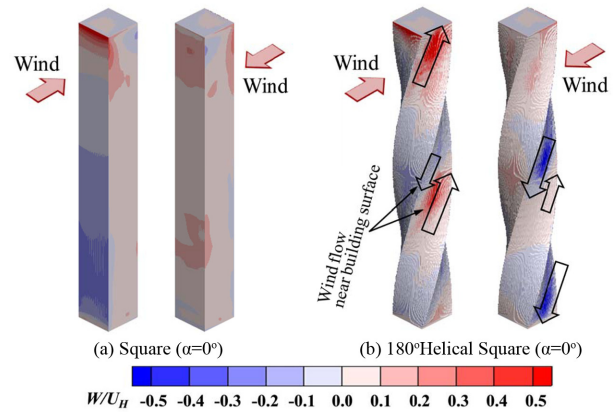


Figure 22. Distributions of mean vertical velocity near building surface.

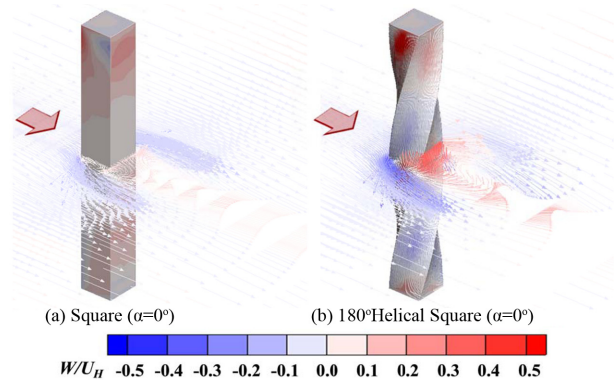


Figure 23. Distributions of mean vertical velocity around building.

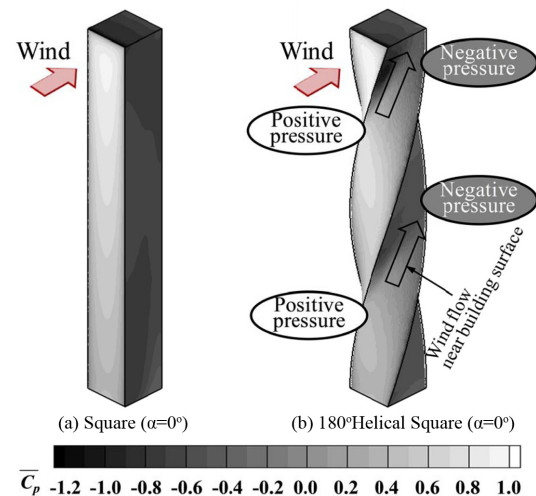


Figure 24. Distributions of mean pressure coefficient.

plicated flow conditions near and around buildings including vertical flows make vortex shedding random or irregular, also resulting in further position of vortex formation from the building's leeward surface.

7. Conclusions

Aerodynamic force measurements, wind pressure measurements and LES (Large-Eddy Simulation) were conducted for tall building models with various building shapes and the same height and volume. Comparison and discussion of the aerodynamic characteristics of tall buildings led to the following conclusions.

(1) For the maximum mean overturning moment coefficients, Tapered models such as 4-Tapered and Setback Models show better aerodynamic behaviors in the along-wind direction, and Corner modification models, Helical models, and Cross Opening models whose opening sizes are $h/H = 11/24$ show better aerodynamic behaviors in the across-wind direction.

(2) For the maximum fluctuating overturning moment coefficients, Corner modification models, 4-Tapered and Setback Models show better aerodynamic behaviors in both along-wind and across-wind directions. Cross Opening Model with $h/H = 11/24$ and the Helical models also show better aerodynamic behaviors in the across-wind direction.

(3) For all building models, the correlations between maximum mean coefficients and maximum fluctuating coefficients are high for both along-wind and across-wind directions. And, the high correlations between maximum mean (and fluctuating) overturning moment coefficients in along-wind direction and those in the across-wind direction are again observed.

(4) The aerodynamic characteristics of the composite models with multiple modifications are mostly superior to those of the models with single modification.

(5) From the response analyses, Corner modification models, Helical models and all composite models show a good performance in safety design. However, Corner modification models and Composite models with tapered modifications have disadvantages in the evaluation of habitability. Conversely, Helical models which does not contain the tapered component show superior aerodynamic behaviors in both safety and habitability design to the Square Model. The design wind load of the 180°Helical models is 70% that of the Square model. Prior to planning the vibration control systems for tall buildings, evaluations of aerodynamic characteristics depending on building shapes are indispensable in tall building projects

(6) For the Square Model, all the vortex components are shed at almost the same time throughout the height, greatly exciting the models in across-wind direction. Contrary to the Square Model, those of the Setback Model and the 180°Helical Square Model vary greatly with height. For those models, because the shedding frequencies of each height are different, the resulting across-wind force decreases correspondingly.

(7) For 180°Helical Square Model, weak vortices with wide-band are shed irregularly throughout the height, and these results in the better aerodynamic behaviors as discussed above.

(8) From the numerical simulations, the vertical flows on the 180°Helical Square Model is more significant than those on the Square Model, encouraging more 3-dimensionality. The vertical flows are assumed to make the vortex shedding random, forming a vortex further from the building surface in the wake.

Acknowledgements

N. Koshika of Kajima Corp., K. Yamawaki of NIKKEN SEKKEI Ltd., Y. Hitomi of NIHON SEKKEI Ltd., Y. Hayano of MAD Tokyo and S. Igarashi of Takenaka Corp. provided us with helpful advice for setting experimental cases. This study comprised part of a project funded by “the Ministry of Land, Infrastructure, Transport and Tourism, Japan” and “the Strategic Japanese-Chinese Cooperative Program on Science and Technology (S&T) for Environmental Conservation and Construction of a Society with Less Environmental Burden (NSFC-JST)”.

References

- Architectural Institution of Japan. (2004a). *Recommendations for Loads on Buildings 2004*.
- Architectural Institution of Japan. (2004b). *Guidelines for the evaluation of habitability to building vibration*.
- Amano, T. (1995). “The effect of corner-cutting of three dimensional square cylinders on vortex-induced oscillation and galloping in uniform flow.” *Journal of Structural and Construction Engineering*, AIJ, 478, pp. 63–69. (in Japanese)
- Cooper, K. R., Nakayama, M., Sasaki, Y., Fediw, A. A., Resende-Ide, S. and Zan, S. J. (1997). “Unsteady aerodynamic force measurements on a super-tall building with a tapered cross section.” *Journal of Wind Engineering and Industrial Aerodynamics*, 72, pp. 199–212.
- Dutton, R. and Isyumou, N. (1990). “Reduction of tall building motion by aerodynamic treatments.” *Journal of Wind Engineering and Industrial Aerodynamics*, 36, pp. 739–747.
- Hayashida, H. and Iwasa, Y. (1990). “Aerodynamic shape effects on tall building for vortex induced vibration.” *Journal of Wind Engineering and Industrial Aerodynamics*, 33(1-2), pp. 237–242.
- Hayashida, H., Mataka, Y. and Iwasa, Y. (1992). “Aerodynamic damping effects of tall building for a vortex induced vibration.” *Journal of Wind Engineering and Industrial Aerodynamics*, 43(3), pp. 1973–1983.
- Kajishima, T. (1999). “Finite-difference method for convective terms using non-uniform grid.” *Journal of the Japan Society of Mechanical Engineers series B*, 65(633), pp. 103–108. (in Japanese)
- Kawai, H. (1998). “Effect of corner modifications on aeroelastic instabilities of tall buildings.” *Journal of Wind Engineering and Industrial Aerodynamics*, 74-76, pp. 719–729.
- Kim, Y. C. and Kanda, J. (2010a). “Characteristics of aerodynamic forces and pressures on square plan buildings with height variations.” *Journal of Wind Engineering and Industrial Aerodynamics*, 98, pp. 449–465.

- Kim, Y. C. and Kanda, J. (2010b). "Effects of taper and set-back on wind force and wind-induced response of tall buildings." *Wind and Structures*, 13(6), pp. 499~517.
- Kim, Y. C., Kanda, J. and Tamura, Y. (2011). "Wind-induced coupled motion of tall buildings with varying square plan with height." *Journal of Wind Engineering and Industrial Aerodynamics*, 99(5), pp. 638~650.
- Kim, Y. C. and Kanda, J. (2013). "Wind pressures on tapered and set-back tall building." *Journal of Fluids and Structures*, 39, pp. 306~321.
- Kim, Y. M. and You, K. P. (2002). "Dynamic responses of a tapered tall building to wind load." *Journal of Wind Engineering and Industrial Aerodynamics*, 90, pp. 1771~1782.
- Kim, Y. M., You, K. P. and Ko, N. H. (2008). "Across-wind Response of an Aeroelastic Tapered Tall Building." *Journal of Wind Engineering and Industrial Aerodynamics*, 96, pp. 1307~1319.
- Kumar, B. E., Tamura, Y., Yoshida, A., Kim, Y. C. and Yang, Q. (2012). "Local and total wind force characteristics of triangular-section tall buildings." *Proc. of the 22nd National Symposium on Wind Engineering*, pp. 179~184.
- Kwok, K. C. S., Wilhelm, P. A. and Wilkie, B. G. (1988). "Effect of edge configuration on wind-induced response of tall buildings." *Engineering Structures*, 10, pp. 135~140.
- Morinishi, Y., Lund, T., Vasilyev, V. and Moin, P. (1998). "Fully conservative higher order finite difference scheme for incompressible flow." *Journal of Computational Physics*, 143, pp. 90~124.
- Miyashita, K., Katagiri, J., Nakamura, O., Ohkuma, T., Tamura, Y., Itoh, M. and Mimachi, T. (1993). "Wind-induced Response of High-rise Buildings." *Journal of Wind Engineering and Industrial Aerodynamics*, 50, pp. 319~328.
- Shiraishi, N., Matsumoto, M., Shirato, H., Ishizaki, H., Osada, M. and Matsui, T. (1986). "On aerodynamic stability effects for bluff rectangular cylinders by their corners cut." *Proc. of the 19th National Symposium on Wind Engineering*, Japan, pp. 193~198. (in Japanese)
- Tamura, A., Kikuchi, K. and Takahashi, T. (1997). "Residual cutting method for elliptic boundary value problems." *Journal of Computational Physics*, 137(2), pp. 247~264.
- Tamura, Y., Nakai, M., Ohtake, K., Koshika, N., Yamawaki, K. and Hitomi, Y. (2011). Study on Wind Resistant Design Method of Super High-rise Buildings with Various Unconventional Configurations, The Ministry of Land, Infrastructure, Transport and Tourism, Japan, <<http://www.mlit.go.jp/tec/gijyutu/kaihatu/josei/067houkoku.pdf>>, accessed 2011/01/17 (in Japanese)
- Tanaka, H., Tamura, Y., Ohtake, K., Nakai, M. and Kim, Y. C. (2012). "Experimental investigation of aerodynamic forces and wind pressures acting on tall buildings with various unconventional configurations." *Journal of Wind Engineering and Industrial Aerodynamics*, 107-108, pp. 179~191.
- Vickery, B. J. and Clark, A. W. (1972). "Lift or across-wind response of tapered stacks." *Proc. of the American Society of Civil Engineers*, 98(ST1), pp. 1~20.
- Werner, H. and Wengle, H. (1991). "Large-eddy simulation of turbulent flow over and around a cube in plate channel." *Proc. 8th Symp. on Turbulent shear Flows*, 19-4, pp. 155~158.